ARTICLE IN PRESS

Hydroxyapatite coatings prepared by a high power laminar plasma jet

Miroljub Vilotijević [a,*], Petar Marković [a], Slavica Zec [b], Slobodan Marinković [b], Vukoman Jokanović [b]

[a] Plasma Jet Co, Branicevska 29, 11000 Belgrade, Serbia
[b] VINCA Institute of Nuclear Sciences, Mike Petrovica Alasa 12-14 Belgrade, Serbia

ARTICLE INFO

ABSTRACT

For two hydroxyapatite (HA) powders, containing particles differing in mass by a factor of 20, a set of optimum deposition parameters was defined, leading to the coatings with high crystallinity (80–90%), high adhesion strength (60 and 40 MPa for the coating thicknesses of 120 μm and 350 μm, respectively) and excellent microstructure (coatings were without micro- or macro-cracks, without delaminating on substrate-coating surface contact, and possess low porosity, 1–2%). It was shown that higher plasma power (52 kW) did not necessarily lead to a higher HA decomposition.

© 2011 Elsevier B.V. All rights reserved.

1. Introduction

Currently, the plasma spray process is the most pervasive technique used to deposit commercially HA coatings on surgical implants. Some of the commercially available plasma spray installations (Table 1), based on the conventional plasma gun (PG), have been used for this purpose. Although this PG construction is the most prevalent on the market the plasma jet thus generated has unfavorable dynamic characteristics.

In the conventional plasma gun, the main factors causing high plasma turbulence are strong voltage and current fluctuations, which are a consequence of the specific cathode/anode configuration. Fluctuations of the arc root along the anode canal create plasma with highly different temperature and speed in both radial and axial directions, as described by Fauchais (2004) and Ghorui and Das (2004). Barbezat and Landes (1999) pointed out to the unfavorable turbulent structure of the plasma jet generated by F4 plasma gun (the most frequently used PG by HA deposition, Table 1). These authors also stated that the plasma jet originating from the PG of the novel construction (Triplex, Sulzer Metco) is characterized as "almost laminar flow".

Moreover, because of the HA tendency to phase transformations at higher temperatures, researchers use very often a lower plasma power, applying plasma spray deposition process. Table 1 presents an overview of the recent results of the HA coatings prepared by different commercial plasma spray installations. Details

of the plasma installation, applied power, as well as the characteristics of the resulting HA coatings are shown, including the phase composition, porosity and adhesion strength. A wide power range (12–45 kW) has been used to deposit plasma sprayed coatings (Table 1). If higher power of the order of 35–45 kW is used, a considerable decomposition of the HA particle occurs, leading to the increased amounts of amorphous HA (ACP), tricalcium phosphate (TCP), tetracalcium phosphate (TTCP) and particularly to an increase of the exceptionally unfavorable CaO phase as established by Sun et al. (2003) and Mohammadi et al. (2008).

McPherson et al. (1995) found out that, total melting of the HA particle can be avoided using the lower power; instead, it is converted to a semi molten state. It is one of the methods used to retain as high as possible the crystal HA/amorphous ACP ratio, counteracting a tendency of the HA ceramics to remain in the metastable glassy phase upon crystallization from the liquid phase as pointed out by Gross and Berndt (1998) and Gross et al. (1998). Thus, the majority of manufacturers of prostheses solve the problem of decomposition of HA particles by using the lower power of plasma and the coarser powder. Such an approach, however, has a drawback. Deposition of the HA coating under the low power regimes and through use of standard commercial anode nozzles (which is the most common case) results also in the lowering of the plasma jet velocity which is proportional to the plasma power as it was shown by Planche et al. (1998).

There are several reasons for the turbulent featured plasma jet being not a suitable one for the plasma spray process. One reason is due to the fact that turbulence leads to a complex trajectory of the particle in the plasma jet, and consequently influences the heat and velocity transfer from plasma to the particles. As Pfender and Lee

Table 1
Overview of used plasma installations, power ranges and characteristics of the deposited HA coatings including phase composition, porosity and adhesion strength.

Plasma installation	Net power (kW)	Phase characteristics	Porosity (%)	Adhesion (MPa)	Reference, year
Metco, USA	37.7	n.a. high ACP, CaO (XRD)	n.a.	13 pure HA 17.3 HA + 60%Ti	Zheng et al. (2000)
PT M1100C, Switzerland	40.2	n.a.	3.5–4.0	2.7–9.2 2.1–8.7	Yang and Chang (2001)
SG-100 Praxair, USA	12	Strong CaO peak, high ACP	18.9	18.5	Khor et al. (2003)
Metco 3MB, USA	27.5–42	Strong CaO peak at 42 kW (XRD)	12–7	n.a.	Sun et al. (2003)
PT M1000, F4 gun	28	65% cryst. HA 35% ACP (XRD data)	"very large pores"	n.a.	Heimann et al. (2004)
Sulzer Metco, F4 gun, VPS	45.2	n.a. except by XRD: low: cryst. HA; high: ACP, TCP, TTCP, CaO	n.a.	4.5–6 (diff. sub.)	Oh et al. (2005)
Metco 3MB	35	HA, TTCP, TCP, ACP, CaO	n.a.	18.1–24.1	Mohammadi et al. (2007)
Metco 3MB	28–36.4	70–55% HA 10.7–13.9% TCP 4.1–6.9% TTCP 4.7–10.9% CaO 10.7–13.2% ACP (low to high power)	10.7–9.1 (low to high power)	n.a.	Mohammadi et al. (2008)

PT—plasma technik, n.a.—not analyzed, VPS—vacuum plasma spraying.

(1985) argued: "The heat and momentum transferred to particles is the integrated time history of all eddies encountered". On the other hand the turbulence is also the cause of the increase of the "externally entrained air and consequently a rapidly decrease of the plasma velocity" (Pfender et al., 1991).

It was shown by Bisson et al. (2003a) and Vardelle et al. (2006), that the plasma turbulence in such PGs is the cause of a high dispersion of particle velocity (of the order of 200 m/s), as well as of particle temperature (of about 600 °C). Bisson et al. (2003b) showed experimentally (with Al_2O_3 powder) that an increase of plasma jet turbulence drastically lowered microstructure quality coating (60% higher porosity, five times higher number of unmelted particles) followed by the considerably lowered deposition efficiency, from 73% to 48%. Due to the low HA density, all this effects may play a relatively significant role even in the case of larger particles. In the case of HA coatings this may lead to a particle overheating followed by dehydration and by higher thermal decomposition leading in turn to increased ratios of ACP, TCP, TTCP, and in particular CaO phases (Table 1).

As a consequence, the HA coating obtained by plasma jet with turbulence properties has often a poor micro structural characteristics (increased porosity, poor cohesion between splats, cracks), which results in poor cohesion/adhesion strength. The problem of losing the cohesion/adhesion strength directs the manufacturers towards the thinner coatings (about 50 μm), because these coatings have proved themselves to be more resistant to delamination. On the other hand, Heimann (2006) indicated an advantage of the thicker coatings (>150 μm) is indicated, because the "thicker coating will be needed to stimulate the bone reconstruction over a longer time". Table 1 shows a wide range of porosity (4–20%) and adhesion (2–24 MPa) of the HA coatings obtained.

An essential requirement for the HA coating is long term stability after implantation. To reach the long term stability (in vitro and in vivo), Yang et al. (1997) proposed that it is more important to have a good coating microstructure (low porosity and high adhesion strength) than crystallinity or absence of impurity phases. Tsui et al. (1998) concluded that a perfect HA coating for implants "would be one with low porosity, strong cohesive strength, good adhesion to substrate, a high degree of crystallinity and high chemical purity and phase stability". With a conventional plasma gun, these properties are hard to achieve because of the unfavorable dynamic characteristics (a very turbulent plasma jet with distinctly heterogeneous distribution of temperature and speed in radial and axial directions) of the plasma jet.

Within the last few years, attempts were made to overcome the problems of poor coatings microstructure by using different PG constructions in the plasma coating process. Using the originally developed technology, gas tunnel type plasma spraying, Morks and Kobayashi (2006) showed that in ranges of plasma power from about 19 to 22 kW, changing the argon flow rate in the range of 100–170 L/min, it is possible to reduce the porosity from 40% to around 4%. The coating's crystallinity is improved at the same time. Kou et al. (2008) got HA coating of good microstructure by using the originally designed PG of a "forced constricted type". Working at a low power within the range from 4 to 6 kW, the significant decomposition of HA particles, with 30 μm powder granulation, could not be avoided. At higher powers, exceeding 5 kW, the strong XRD reflection of the CaO phase was recorded, followed by the increased coating adhesion.

The present paper presents the HA coating characteristics obtained by the atmospheric plasma spray procedure using a PJ-100 plasma installation. Vilotijevic et al. (2009) documented that the plasma jet generated with this installation has considerably better characteristics of flow laminarity, temperature homogeneity, and higher plume velocity than that generated by the conventional PG. Fig. 1 shows the shape and texture of the plasma plume generated by PJ-100 installation. The picture was obtained using an ultrahigh speed camera (Imacon 760 with a speed of 10^6 frames/s).

Specific characteristics of this plasma are its unusually long plume (70 mm; i.e. twice the plume length of the conventional PG), high radial and axial plasma temperature homogeneity (evident from the brightness distribution), as well as the laminar plasma flow along 2/3 of its length from the anode nozzle exit. The first difference between the plasma jet which is generated by PJ-100 installation and the one derived by the conventional PG can be seen in terms of plasma velocity. The PJ-100 plasma velocities, measured at its very end in the zone of 60–70 mm from anode nozzle exit, were 1500–1800 m/s (Vilotijevic et al., 2009). At the same distance from the anode nozzle exit, the plasma jet velocities of the conven-
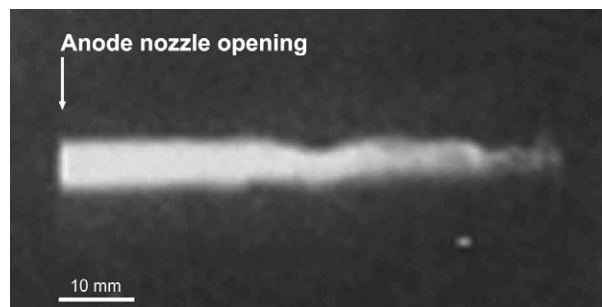

Fig. 1. Shape and texture of the plasma plume exiting the PJ-100 anode nozzle.

tional PG were determined to be about 200–400 m/s for the power range of 11–24 kW, respectively, as reported by Dyshlovenko et al. (2004).

In this study the most important characteristics of the HA plasma coating (phase composition, porosity, adhesion and microstructure) have been measured for a range of deposition parameters. This has been done for two different granulations chosen so that their mean particle mass differs by a factor of 20.

2. Materials and methods

The plasma installation PJ-100 (Plasma Jet, Serbia) was used for the plasma spray process. Basic parameters of the installation used for the coating deposition are presented in Table 2.

Two commercially available HA powders with different granulations were used: HA powder, XPT-D-703 (Sulzer Metco, USA), with a mean particle size, ca. 33 μm (hereinafter referred to as the "finer powder"), and HA powder Captal 90 (Plasma Biotal, UK), with an average granulation of 90 μm (hereinafter referred to the "coarser powder"). Data on the granulation of the powders used were obtained from the manufacturer's specifications. The coatings were deposited on plates (25 mm × 50 mm × 3 mm) and specimens for mechanical testing ($\varnothing$ 25.0 mm × 70 mm) were made of SS AISI 316 LVM material. Both plates and specimens were mounted on a disk $\varnothing$ 200 mm rotating at 3.7 rev/s. The complete coating process was performed in two to three short intervals from 7 to 10 s each, with the brake rate of few minutes between the cycles. A standard procedure of sand blasting with corundum particles of 2 mm preceded the deposition. The realized surface roughness (Ra) was in the range from 4.72 to 5.28 μm (Perthen Perthometer).

Optical microscopy examination was performed using a Zeiss Axiovert microscope. After cutting, specimens were mounted in the cold-polymerizing mass (PMMA). The specimens were first ground with sand paper, granulation # 80, 220, 360, 600, and then were polished with a diamond paste (granulation <2 μm). The final polishing was performed with Al_2O_3 polishing paste (granulation 0.25 μm).

Adhesion strength was measured according to the ASTM C 633 standard using an Instron 1185 machine for mechanical testing with bridge velocity of 2 mm/min. Usually five specimens were tested, except for a few experiments in which deposition was made on six specimens, as discussed below. We used the Klebbi adhesive (Metco, USA) polymerizing for 2 h at 180 °C. Our measurements gave the adhesive strength of 86.1 ± 3.4 MPa ($n = 10$).

X-ray diffraction (XRD) patterns were recorded in the range 20–60° 2Θ on a Siemens D500 diffractometer using Cu Kα1 radiation (angular steps 0.02° with step time of 1 s). Quantitative analysis was made by the external standard method, according to the ASTM F 2024-00 standard. The RIR and I_{rel} coefficients were experimentally determined. RIR was assessed from 50:50 mass mixture of the initial HA powder and α-Al_2O_3 standard as a mean value of three measurements. The amorphous phase (ACP) ratio was obtained by subtracting the sum of all the detected crystalline phases from 100%. The estimated relative error of the quantitative XRD method was ±7%. The crystallinity index (Ic) was estimated from the ratio of intensity of all crystalline peaks and the total surface area of the X-ray pattern within the 20–40° 2Θ range.

The coating porosity as well as the ratio of partially melted particles was estimated from the respective micrographs using VIDAS software. Five micrographs with magnification 500× were used for each porosity determination.

3. Results

The results of the analysis of the cross-sectional morphology of coatings together with the results of quantitative analysis of phases present in coatings are reported, as well as measurements of bond strength of coatings obtained using "finer" and "coarser" powders in the process of plasma spraying.

3.1. Cross-sectional morphology

The results of cross-sectional morphology of coatings obtained using "finer" (Section 3.1.1) and "coarser" powders (Section 3.1.2) are presented in this chapter.

3.1.1. The microstructure of the "finer" powder coating

Fig. 2 shows microstructure of the coatings (and the corresponding XRD pattern) deposited using finer powder (33 μm) at substrate temperature (T_s) 15 °C and two stand-off distances (SOD), SOD = 80 mm and SOD = 150 mm. The substrate temperature in this study is the initial substrate temperature.

According to the XRD patterns presented in Fig. 2, an increase of SOD is followed by an appearance of the ACP (amorphous hump) and a slight increase of the CaO phase. The same tendency was established by Sun et al. (2003) and Mohammadi et al. (2008).

According to the micrographs, both coatings have similar structural characteristics. There are no macro cracks, and the coatings have low porosity and consist of a matrix (light zone) in which "grey" zones are relatively homogeneously distributed. On the magnified detail of the coating, Fig. 3a, it is clearly seen that the grey phase (G) is neither a pore nor a non molten particle, but rather the core of an incompletely molten particle, somewhat deformed by hitting the substrate. Therefore the contact of the grey zone with the matrix is excellent, without micro cracks. There is also a slight porosity (P) formed primarily due to captured air pockets on the boundaries of the splats (Fig. 3a). The size of the visible pores is of the order of a few μm^2.

Fig. 3b shows the microstructure of the coating, shown in Fig. 2a, etched in 1% HNO_3 for about 4 s. A laminated structure of the coating is visible, with excellent boundaries between the splats, without micro cracks or pores. No globular structure is visible in the etched coating, suggesting that there are virtually no non molten particles, although a high mass input of the powder (2 g/s) was used.

Quantification of the partly molten particles (grey phase) ratio and of the porosity in the coatings deposited at different SOD was made, Table 3.

For all the investigated SODs, the partly molten particle ratio is practically constant, about 9%. Coating porosity is about 1–2%, while at a distance of 80 mm minimal porosity of about 0.5% was found.

The fact that the partly molten particle ratio is practically constant in the investigated SOD range could be probably the con-

Table 2
Parameters of the PJ-100 installation during the HA deposition process.

Power (kW)	52.0 ± 1.5
Voltage (V)	120 ± 2
Current (A)	430 ± 5
Argon flow (L/min)	38.5 ± 1.2
Nitrogen flow (L/min)	28.2 ± 1.0
Powder carrier gas, air (L/min)	8
Powder mass input (g/s)	2.0 ± 0.1

Table 3
Partly molten particle ratio and porosity as a function of SOD for the coatings prepared from finer powder.

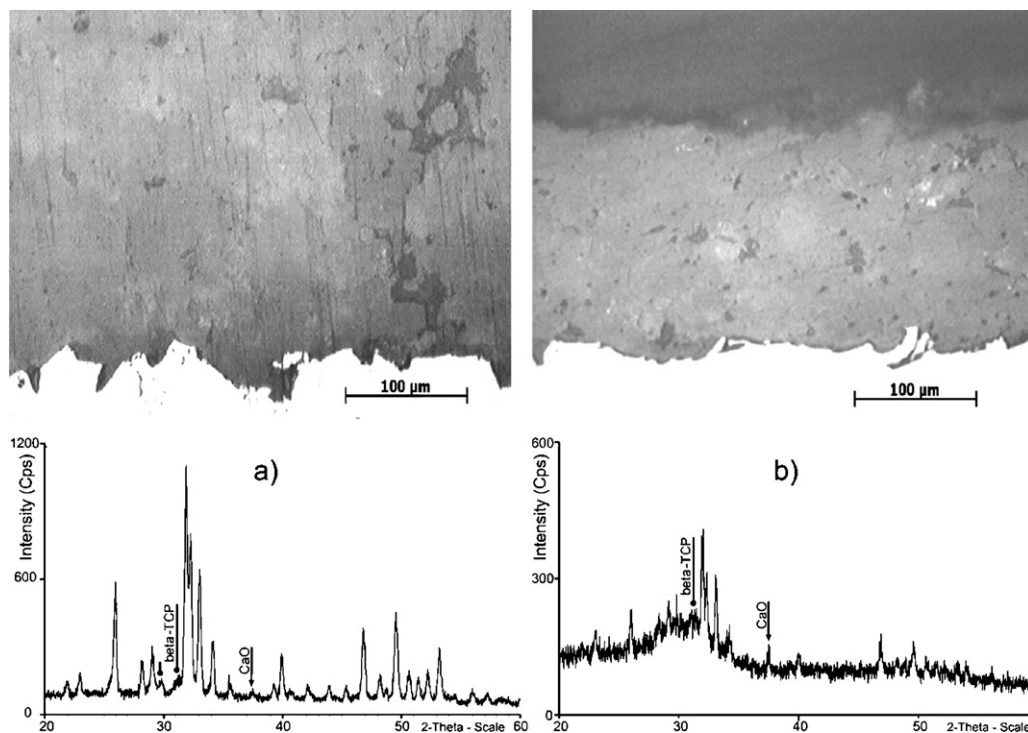| Standoff distance (mm)	Partly molten particle ratio (%)	Porosity (%)
80	9.7 ± 1.3	0.4 ± 0.1
100	6.5 ± 2.6	1.5 ± 0.8
150	9.0 ± 1.3	1.4 ± 0.4

Fig. 2. (a) Optical micrographs of the coatings prepared using finer powder at SOD = 80 mm and (b) SOD = 150 mm with the respective XRD patterns.
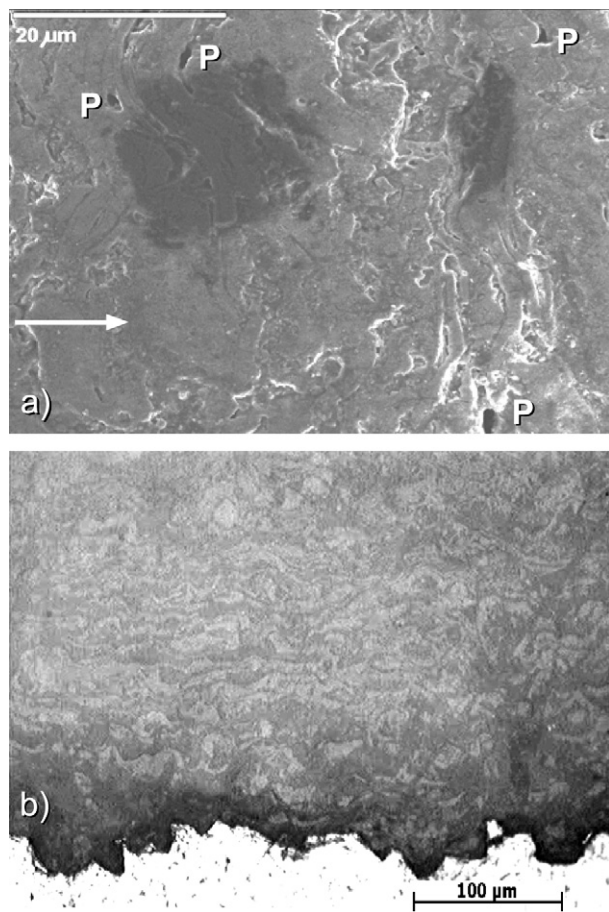

Fig. 3. (a) SEM detail of the "grey" phase (G) presented in Fig. 2a (the arrow shows spraying direction), (b) microstructure of the coating deposited at SOD = 80 mm, after etching with 1% HNO_3.

sequence of the used constant power level and of the constant powder mass input. Although microstructures of the coatings prepared from the finer powder in the SOD range of 80–150 mm are very similar to each other, their phase compositions are quite different, as follows from the XRD patterns (Fig. 2a and b).

3.1.2. The microstructure of the "coarser" powder coating

The micrograph of the coating obtained from the coarser powder at SOD = 80 mm is presented in Fig. 4a, while Fig. 4b illustrates the etched coating. The estimated grey phase ratio in these coating amounts to 13.6%, and its porosity is 1.1%. The coating has a very compact structure with minimum porosity, without macro cracks, and with an excellent boundary layer between the coating and the substrate, without any delamination.

The micrograph of the etched coating shows exceptional stability towards 1% HNO_3. While the coating/substrate boundary for the finer power was strongly etched (Fig. 3b), the micrograph of the coating prepared from the coarser powder does not show any increased solubility in the coating/substrate boundary zone (Fig. 4b). Moreover, this coating remained almost unchanged after etching. The zones where etching is faster correspond to the zones with phase impurities, especially those with ACP. The micrograph of the etched coating prepared from the coarser powder indicates a low ACP phase content, even on the surface of the molten particle in the jet, which is suggested by the fact that the etching can hardly outline the contour of the splats. The exceptional stability of the coating prepared from the coarser powder in the etching process indicates it's high crystalline HA phase content.

Fig. 5 shows that the XRD patterns of the coarser particles and of the corresponding coatings are practically identical, except for the minor peaks arising from the new phases formed during the deposition. The quantitative analysis of the phases presented in the coatings obtained with the finer and coarser powder (Table 4) shows that the coating prepared from the coarser powder contains predominantly HA in crystal phase with low amount of amorphous phase.
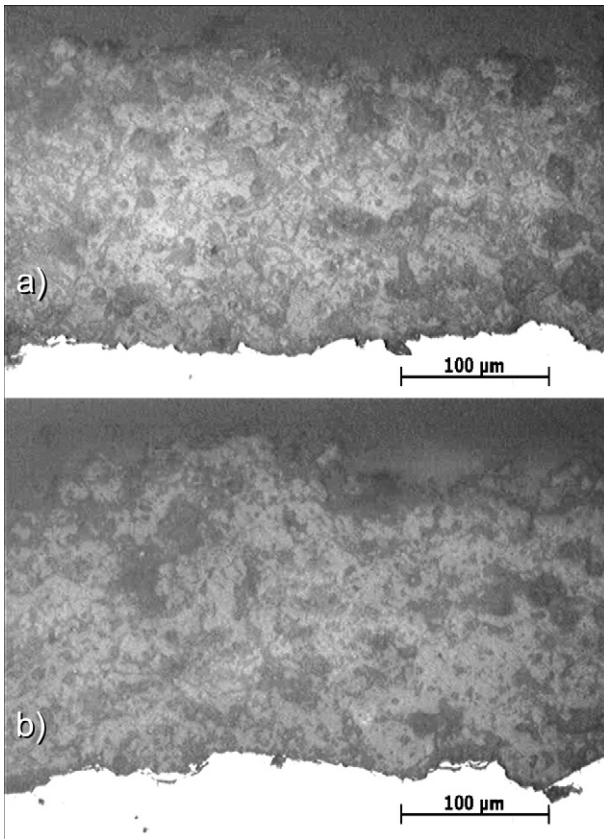
Fig. 4. Microstructure of the coating prepared from the coarse powder, as-deposited (a) and etched (b).

3.1.3. The phase composition of the "finer" and the "coarser" powder coatings as a function of SOD and T_s

Analysis of the XRD patterns reveals that crystalline phases HA, β-TCP and CaO are detected in the coatings, along with a corresponding ratio of the amorphous HA phase (ACP). The latter being indicated by the broad and rather symmetrical band centered around 31° 2Θ. According to the literature, the crystallinity index was estimated for different 2Θ ranges, from 20–37° 2Θ, McPherson et al. (1995), to 25–40° 2Θ, Auclair-Daigle et al. (2005). The 20–40° 2Θ range was chosen here because in the XRD pattern indicating maximum ACP phase content for the "finer" powder coating (Fig. 2b), the amorphous band appears in this range. Gross et al. (1998) also used the same range. Table 4 presents results of the quantitative analysis of the XRD patterns for the coatings prepared at different SODs.

Table 4 shows the estimated crystallinity index (Ic), and concentrations of the crystalline phases and ACP phase for the coatings prepared from the two investigated powders.

Changes in the phase composition of the coatings prepared from both granulations, is mostly reflected in the crystalline HA phase/ACP phase ratio, while concentrations of both TCP and CaO phases are practically constant in the experimented SOD range. The HA/ACP ratio for the coating prepared from the finer powder is particularly sensitive to SOD. Even during the short time needed for passing the additional 20 mm, namely from SOD = 80 to SOD = 100, a coating of considerably lower crystallinity was formed, while the ACP phase ratio increased.

The coating from the "coarse" powder has considerably more stable composition within the experimented SOD range, showing a very small change in the HA and ACP phase content. There is a considerably higher content of the crystalline HA phase, too. Even at SOD = 150 mm the coating made of the coarse particles has excel-
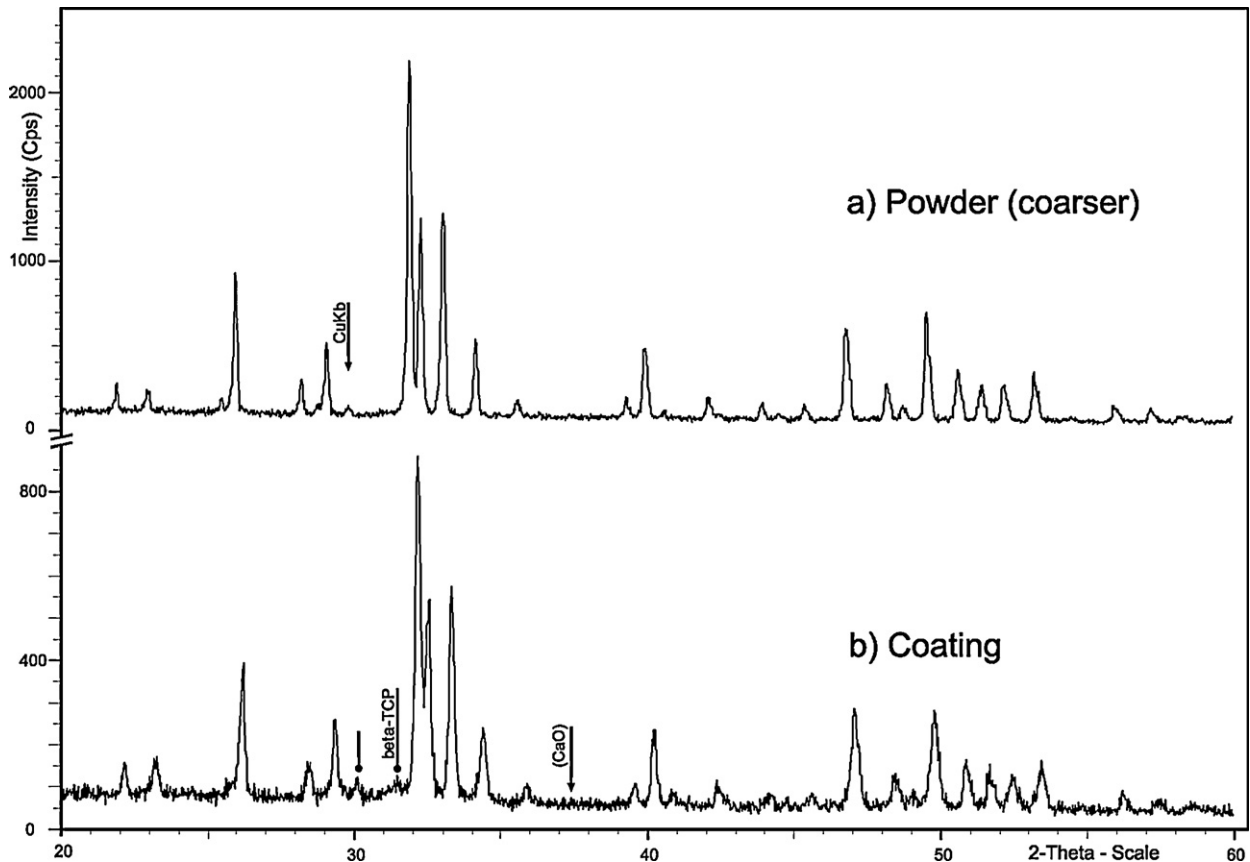

Fig. 5. XRD patterns of the coarse powder (a) and coating (b) deposited at SOD = 80 mm, T_s = 200 °C.

Table 4
Phase composition of the coatings as a function of SOD for finer and coarser particles ($T_s = 200\,°C$).

Powder	SOD (mm)	Ic (%)	HA (%)	β-TCP (%)	CaO (%)	ACP (%)
Finer	80	78.9	53.3	15.0	1.7	30.0
	100	59.1	41.3	7.3	1.1	50.3
	150	37.0	34.1	7.8	2.0	56.1
Coarser	80	83.2	82.6	7.3	0.7	9.4
	100	80.5	71.5	7.8	0.7	20.0
	150	78.6	69.4	4.9	0.7	25.0

lent phase purity with a considerably higher crystalline phase ratio than the coating prepared from the fine powder at SOD = 80 mm.

Increasing substrate temperature is of particular interest for the HA coating, because it is one of the techniques for diminishing particle cooling rate upon collision with the substrate. Diminished cooling rate should lead to an increase of the HA/ACP ratio, due to the longer time available for HA phase re-crystallization from ACP. We have followed the effect of substrate temperature (T_s) in the range from 15 to 200 °C on phase composition of the coatings deposited at SOD = 80 mm for finer and coarser powders, respectively, Table 5.

Effect of substrate temperature on the coating phase composition is practically negligible, in the case of the "finer" powder (within the margin of measurement error). In the case of the "coarser" powder, at the temperature range from 15 to 200 °C, the crystalline HA phase decreases and ACP phase grows, while the TCP and CaO phase ratios remain practically constant. In both cases, collision of the particle with the hotter substrate results in a diminishing particle cooling rate and prolongation of the recrystallization process. This process is not much affected in solidification of the melted particle of the "finer" powder in range of substrate temperatures (T_s) researched.

However, behavior of the coarser particle during its solidification may seem somewhat surprising because prolongation of the crystallization process leads to an increasing amorphous phase ratio. An analysis of these results, followed by a possible explanation will be presented in Section 4.

3.2. Bonding strength measurement

3.2.1. Bonding strength of the "finer" powder coating

We measured the adhesion of the coatings prepared using finer powder at SOD = 80 mm. Within this SOD range, phase composition is suitable for preparation of implants, i.e. crystalline HA ratio > 45% (according to the ASTM F 1185-03 standard). Due to high powder mass input (2 g/s) and oscillatory movements of the plasma gun (about ± 25 mm with respect to the specimen centre) the greatest thickness during deposition is invariably obtained in the middle of the specimen. We therefore produced coatings 400–500 μm thick which, when sanded flat, were reduced to a uniform thickness of 300 μm. The grinding was done with sandpaper #80 and a tool which keeps the ground surface at 90° with respect to the specimen axis.

However, the used adhesive had insufficient adhesion to the coating surface prepared by this procedure. Fig. 6a shows the typical appearance of a specimen surface prepared and broken.
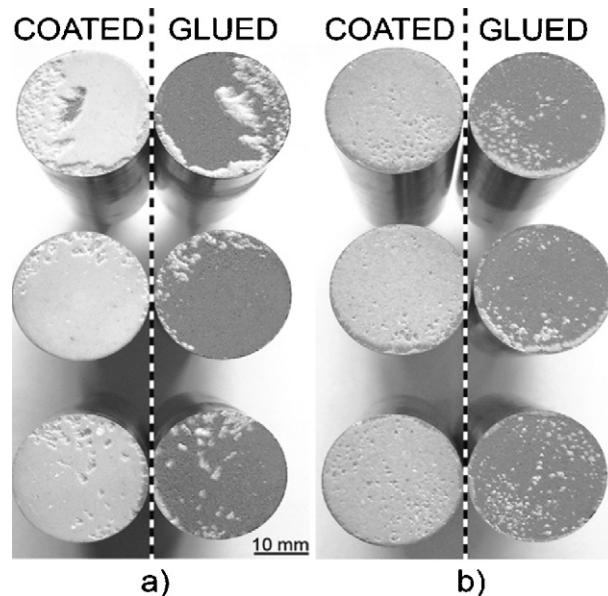

Fig. 6. Fractographs of specimens, SOD = 80 mm, $T_s = 200\,°C$. (a) Finer powder, coating surface flattened, coating thickness 280 ± 14 μm. (b) Coarser powder, as-deposited coating surface, coating thickness 260–290 μm.

For the coatings prepared from both finer and coarser particles, the left side of the figure shows the coated surface and the right shows the glued surface. The broken surfaces are oriented along their axis of reflection. Although the measured adhesion strength for the coating prepared with the finer powder is excellent (41.9 ± 2.0 MPa ($n = 10$)), Fig. 6a clearly shows that the coating remained almost completely on the coated surface, indicating that the separation occurred on the adhesive/HA boundary.

Adhesion of the coating glued with the as-sprayed surface gives slightly lower adhesion values from 31.2 ± 5.0 ($n = 15$). This is understandable in view of the coating surface "curvature", and therefore more unequal allocation of the breaking force, in regard to the flattened surface. In a total of 25 measurements made on the "finer" powder coating (flattened + as-sprayed), the real braking adhesive mode appeared twice only. The certain adhesion strengths were 56.1 MPa (for the as-sprayed surface), and 54.4 MPa (for the flattened surface).

Table 5
Phase composition of coatings prepared from finer and coarser powder at different substrate temperatures (T_s), SOD = 80 mm.

Powder	T_s (°C)	Ic (%)	HA (%)	β-TCP (%)	CaO (%)	ACP (%)
Finer	15	62.0	44.0	8.8	1.2	46.0
	100	65.5	44.9	13.0	2.1	40.1
	200	67.3	48.8	12.6	2.1	36.5
Coarser	15	92.9	91.0	4.4	1.0	3.6
	100	86.0	87.1	6.8	0.4	5.8
	200	83.2	82.0	6.8	0.4	10.8

Table 6
Effect of metallization of the HA coating on adhesion strength and breaking mode.

Coating structure	Adhesion (MPa)	Breaking mode
HA coating	30.2 ± 6.1	Adhesive/HA
HA coating + Mo	46.5 ± 1.7	Cohesion

3.2.2. Bonding strength of the "coarser" powder coating

Adhesion of the coatings prepared from the coarser powder indicate a similar problem—the impossibility of separation of the coatings from the substrate. Fig. 6b shows the typical appearance of the broken surface of specimens obtained from the coarser powder, glued with as sprayed surface. Only small, point-like fragments of the coating pulled by the adhesive occurred in all 15 specimens glued by this method. At SOD = 80 mm, a mean value of adhesion strength of 33.0 ± 7.6 MPa (n = 15) was obtained for coatings 250–300 μm thick. This value is very close to that obtained for breaking of the coatings prepared with finer powder, which were obtained by gluing the as-deposited surface (31.2 MPa). This value is apparently the adhesion limit of used adhesive for the HA surface, which is determined by characteristics of the HA coating (roughness, composition) and by wetting characteristics of the adhesive on the HA surface.

Attempts were made to solve the problem of adhesion of the glue with the coating surface in an original manner, namely by the metallization of the HA coating surface; a better wetting of the glue on the metallic top layer was expected. A thin molybdenum layer was deposited using the plasma spray process. The molybdenum (Metco 64 powder) deposition was performed in a very short time of only 4 s, to avoid the undesirable thermal stress of the basic coating. Nevertheless, it was sufficient to form a molybdenum coating 20–30 μm thick on the HA coating (Fig. 7). Fig. 7 shows that the Mo top coating adheres well to the HA coating, forming a dense non-porous coating which completely fills the unevenness of the HA coating.

The effect of HA surface metallization on adhesion strength is well illustrated by a data presented in Table 6. In one experiment, six specimens were coated to a thickness of 275 ± 15 μm (mean value) using the coarser powder at SOD = 80 mm. Three of the six specimens were then metallized. The data presented in Table 6 clearly show that the effect of the top layer is substantial: breaking strength is increased by approximately 50%. However, more impor-
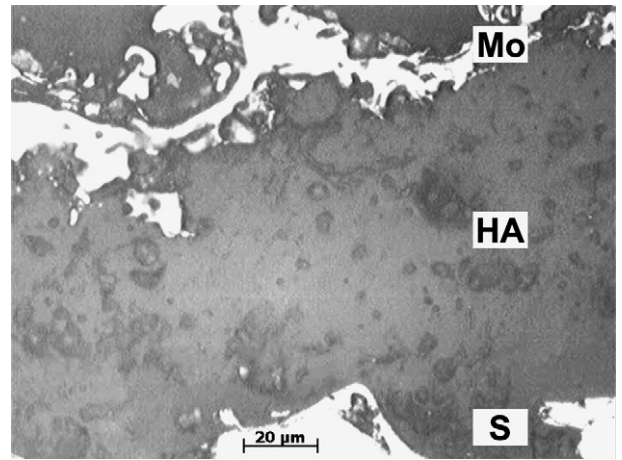

Fig. 7. The HA coating prepared from coarse powder metallized by depositing a top Mo layer.

tantly, for the first time, the breaking mode was clearly defined, i.e. cohesion in this case.

The metallization of the HA surface enabled an estimate of the breaking force for thinner coatings. The ASTM C 633 standard does not allow adhesion measurements for thinner coatings, of the order of 50 or 100 μm. However, adhesion measurements described in the literature are commonly performed in this range. The problem with adhesion measurements of thin coatings is the possible penetration of adhesive through pores and cracks in the layer. In this study, obtained coatings were free of macro cracks and possessed minimal closed porosity, so that adhesive penetration to the substrate was not expected. Furthermore, the presence of a metallic non-porous top coating guaranteed that penetration of the adhesive had not occurred.

Fig. 8a presents adhesion strength of coatings prepared from the coarser particles at T_s = 200 °C, as a function of mean thickness. Mean coating thickness was estimated from thickness measurements using the micrographs of the coating cross section, taking the mean value from 30 readings. Values of the mean thickness ranged from 120 ± 15 μm to 350 ± 20 μm.

Adhesion strength decreases with increasing coating thickness probably as a consequence of residual stresses in the coating.
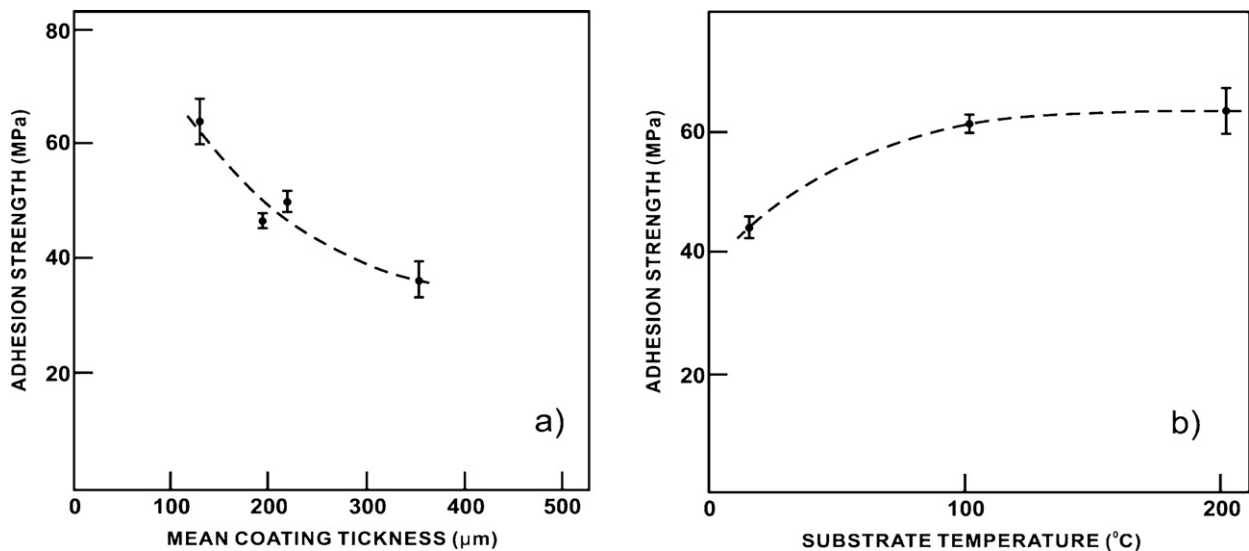

Fig. 8. Adhesion of the coating prepared from the coarser powder as a function of: (a) coating thickness, T_s = 200 °C; (b) substrate temperature, mean coating thickness = 120 ± 20 μm.

For coatings with a thickness of about 120 μm, most often used for implant applications, excellent adhesion (over 60 MPa) was obtained.

These high adhesion values are a result of the dense non-porous structure of the coatings. Upon microscopic examination of the coating cross sections of plates and specimens deposited in the same experimental cycle, no macro cracks or coating delamination were observed. Therefore, a high bond strength value was not surprising, nor was the observed cohesion breaking mode. The coating made of the coarser powder shows not only phase stability, but also constant adhesion strength for SOD of 80–150 mm. In another series of experiments, undertaken to obtain more data directly related to implant application, it was found that adhesion strength of coatings about 120 μm thick ranges from 63.7 ± 8.7 MPa to 57.3 ± 8.6 MPa for SOD values from 80 mm to 150 mm.

Substrate temperature dependence on adhesion strength of the coatings prepared from the coarser powder was also investigated. Fig. 8b shows the results for substrate temperature ranges of 15–200 °C and coating thicknesses 120 ± 20 μm. Within the T_s range 15–200 °C, an increase of adhesion strength can be noticed (Fig. 8b). Presumably, this increase in adhesion strength is a consequence of diminished stresses on the coating/substrate contact resulting from different thermal expansion coefficient values. It is interesting that the authors Yang and Chang (2001) have noticed the opposite, namely a decrease of adhesion force from 9.18 MPa to 2.73 MPa, for the range of the initial substrate temperature from 50 to 250 °C, respectively. The authors Yang and Chang (2001) explained this by the residual stress increase in the coating itself, as a result of the coating overheating (400 °C, as the final temperature), compared with the initial substrate temperature (T_s).

It is interesting to note that for deposition of coatings from the coarser powder, a compromise in deposition parameters should be made, as an increasing T_s leads to adhesion improvement, but induces a certain decrease of crystallinity (Table 5).

4. Discussion

McPherson et al. (1995) reported that the existing plasma spraying techniques are mainly intended to form a coating made of semi-molten particles with a considerable ratio of non-molten particles. A correlation between HA phase crystallinity and the semi-molten particle content in the coating was documented by Chen et al. (1994).

However, in the present study, such a correlation was not found in our coatings. The coatings prepared from the finer powder (Figs. 2 and 3b) were formed mainly by fully molten particles. Although the semi-molten particles ratio remains practically constant (about 9%) within the investigated SOD range (Table 3), phase composition of the coatings (Table 4) clearly distinguishes coatings deposited at different SOD, with drastically decreasing the HA/ACP ratio with increasing SOD. This result indicates that the crystalline HA phase ratio is not a function of the partly molten particles content (or non-molten, which have not been detected in our coatings in a significant amount).

This means that it is possible to get the coating of an excellent phase composition, with extremely high plasma power (52 kW) and even with the use of finer powder granulation (33 μm) (for SOD = 80 mm, Table 4). Characteristically, for the both powder granulations used, the change in the phase composition is primarily reflected in the crystalline HA/ACP ratio, while composition of other phases detected (TCP, CaO) remains more or less constant within the examined SOD range (Table 4). From Table 4, it can be seen that an increase of the SOD is followed by the increase of the ACP phase, especially in the case of fine powder. It can be concluded that an increase of the particles time in-flight (increased SOD) as well as

the using the finer powder granulation, lead directly to the lowering in the crystallinity of the coating followed by an increase of the ACP phase amount. The phase composition of the coating obtained using the coarser particles powder, presented in Table 4, indicates a low thermal decomposition of the particles in the plasma. In particular, it is obvious on the base of the low TCP phase values in the coating (about 6–7%) and of the particularly low CaO concentrations (<2% for coatings obtained from the finer powder and <1% for coatings from the coarser powder). Appearance of CaO is a consequence of a high HA decomposition degree, Cihlar et al. (1999). Mohammadi et al. (2008) pointed out that the presence of the impurity phases, especially CaO, could significantly influence the overall solubility of HA coatings. From this point of view the coating made of the coarser powder is a better choice. This coating has also very good microstructural characteristics as well as the adhesion strength. The influence of the substrate temperature, in the range of 15–200 °C (Table 5), on the coating characteristics is investigated. The ACP phase fraction of the coating obtained with the finer powder decreases with the increasing T_s, what is in the accordance with the results obtained by Gross et al. (1998). The opposite behavior of the coarser powder coating is found: prolongation of the crystallization process leads to an increasing amorphous phase ratio (Table 5). One of the possible explanations lies in the competition between the recrystallization and dehydration processes. Wang et al. (2004) and Cihlar et al. (1999) confirmed that the first step in the decomposition process is dehydroxylation, starting at about 800–900 °C thus forming oxyhydroxyapatite (OHA). The loss of water from the HA is a dominant reaction up to about 1350 °C, when OHA decomposition begins to form TCP and CaO, with further loss of water in the range of 1350–1477 °C (Cihlar et al., 1999). Both reactions are controlled by water diffusion through molten HA particles. So, collision of a particle 20 times larger results in a larger lateral spreading of the droplet. This, in turn, leads to a considerable increase of surface area and thinning of the still incompletely solidified particle. The diffusion process is faster, with the diffusion time proportional to $[\text{path}]^2$. As a result, more water is removed before solidification. Therefore, the ACP ratio increases with increasing T_s for the coarser powder.

In the paper is shown that there is only small difference in the microstructure and adhesion strength of the coatings prepared with both the finer and the coarser particles. Both coatings are dense, practically non-porous, and are without micro and macro cracks, while their adhesion strength is exceptionally high.

All the results presented suggest, that in the plasma of about 52 kW power, applied in the coating process, the transfer of the heat and the momentum to the particles occurs efficiently (the coatings are formed cooling of the particles molten to a high extent). The efficient fusion of the particles does not considerably influence the phase purity and the crystallinity of the coating (for finer powder coating at SOD = 80 mm and for the coarser powder coating practically in the whole SOD region from 80 to 160 mm). This implies that the particle dwell time in the plasma as well as the time in-flight of the particles to the substrate is short enough to avoid considerable thermal decomposition.

It could be supposed that the use of the plasma jet applied in this work, as plasma with homogeneous distribution of temperature and velocity along both radial and axial directions, with more laminar plasma flow (Fig. 1), followed by considerably higher velocity (as discussed in Section 1), enables the formation of the high quality coating.

5. Conclusion

Plasma sprayed HA coatings were prepared using the high power (about 52 kW) plasma jet with laminar flow. The most

important characteristics of the HA plasma coating (phase composition, porosity, adhesion and microstructure) have been measured for a range of deposition parameters. This has been done for two different granulations chosen so that their mean particle masses differ by a factor of 20. The results obtained are summarized as follows:

- The coatings obtained from finer and coarser powders are characterized by excellent microstructure (coatings are without micro- or macro-cracks, without delamination on the substrate-coating contact surface). Dense coatings having low porosity (about 0.4% for the finer and up to 1.1% for the coarser powder) have been prepared. An important characteristic of the microstructure obtained is the high amount of fully molten particles (about 90%).
- It is possible to prepare coatings with high crystallinity (>80–90%) and good phase composition for finer powder at SOD = 80 mm, and for coarser powder in the whole investigated SOD range. An increase of the substrate temperature from 15 to 200 °C leads to the decrease of the amorphous phase fraction from 46% to 36% for the finer powder coating but to the increase for the coarser powder coating from 4% to 11%.
- The adhesion strength obtained was 54–56 MPa for the coatings 300 μm in thickness prepared from the finer powder. For the coarser powder, dependence of adhesion on the coating thickness and temperature was also examined. It was shown that for relatively thin coatings (about 125 μm) at the substrate temperature 200 °C, adhesion strength was measured at >60 MPa.

Acknowledgments

References

Auclair-Daigle, C., Bureau, M.N., Legoux, J.G., Yahia, L.H., 2005. Bioactive hydroxyapatite coatings on polymer composites for orthopedic implants. J. Biomed. Mater. Res. 75A, 398–408.

Barbezat, G., Landes, K., 1999. Plasma torch-system triplex: increased production and a more stable process. Sulzer Tech. Rev. 4, 32–35.

Bisson, J.F., Gauthier, B., Moreau, C., 2003a. Effect of plasma fluctuations on in-flight particle parameters. J. Therm. Spray Technol. 12, 38–43.

Bisson, J.F., Gauthier, B., Moreau, C., 2003b. Effect of direct-current plasma fluctuations on in-flight particle parameters: Part II. J. Therm. Spray Technol. 12, 258–268.

Chen, J., Wolke, J.G.C., deGroot, K., 1994. Microstructure and crystallinity in hydroxyapatite coatings. Biomaterials 15, 396–399.

Cihlar, J., Buchal, A., Trunec, M., 1999. Kinetics of thermal decomposition of hydroxyapatite bioceramics. J. Mater. Sci. 34, 6121–6131.

Dyshlovenko, S., Pateyron, B., Pawlowski, L., Murano, D., 2004. Numerical simulation of hydroxyapatite powder behaviour in plasma jet. Surf. Coat. Technol. 179, 110–117.

Fauchais, P., 2004. Understanding plasma spraying. J. Phys. D: Appl. Phys. 37, R86–R108.

Ghorui, S., Das, A.K., 2004. Origin of fluctuations in atmospheric pressure arc plasma devices. Phys. Rev. E 69, 7, 026408.

Gross, K.A., Berndt, C.C., 1998. Thermal processing of hydroxyapatite for coating production. J. Biomed. Mater. Res. 39, 580–587.

Gross, K.A., Berndt, C.C., Harman, H., 1998. Amorphous phase formation in plasma-sprayed hydroxyapatite coatings. J. Biomed. Mater. Res. 39, 407–414.

Heimann, R.B., 2006. Thermal spraying of biomaterials. Surf. Coat. Technol. 201, 2012–2019.

Heimann, R.B., Schurmann, N., Muller, R.T., 2004. In vitro and in vivo performance of Ti6Al4V implants with plasma-sprayed osteoconductive hydroxylapatite-bioinert titania bond coat "duplex" systems: an experimental study in sheep. J. Mater. Sci.: Mater. Med. 15, 1045–1052.

Khor, K.A., Gu, Y.W., Quek, C.H., Cheang, P., 2003. Plasma spraying of functionally graded hydroxyapatite/Ti-6Al-4V coatings. Surf. Coat. Technol. 168, 195–201.

Kou, M., Toda, T., Fukumasa, O., 2008. Production of fine hydroxyapatite films using the well-controlled thermal plasma. Surf. Coat. Technol. 202, 5753–5756.

McPherson, R., Gane, N., Bastow, T.J., 1995. Structural characterization of plasma-sprayed hydroxyapatite coatings. J. Mater. Sci.: Mater. Med. 6, 327–334.

Mohammadi, Z., Ziaei-Moayyed, A.A., Mesgar, A.S., 2007. Grit blasting of Ti–6Al–4V alloy: optimisation and its effect on adhesion strength of plasma-sprayed hydroxyapatite coatings. J. Mater. Process. Technol. 194, 15–23.

Mohammadi, Z., Ziaei-Moayyed, A.A., Mesgar, A.S., 2008. In vitro dissolution of plasma-sprayed hydroxyapatite coatings with different characteristics: experimental study and modeling. Biomed. Mater. 3, 7, 015006.

Morks, M.F., Kobayashi, A., 2006. Influence of gas flow rate on the microstructure and mechanical properties of hydroxyapatite coatings fabricated by gas tunnel type plasma spraying. Surf. Coat. Technol. 201, 2560–2566.

Oh, I., Nomura, N., Chiba, A., Murayama, Y., Masahashi, N., Lee, B., Hanada, S., 2005. Microstructures and bond strengths of plasma-sprayed hydroxyapatite coatings on porous titanium substrates. J. Mater. Sci.: Mater. Med. 16, 635–640.

Pfender, E., Lee, Y.C., 1985. Particle dynamics and particle heat and mass transfer in thermal plasmas. Part 1. The momentum of a single particle without thermal effects. Plasma Chem. Plasma Process. 5, 211–237.

Pfender, E., Fincke, J., Spores, R., 1991. Entrainment of cold gas into thermal plasma jets. Plasma Chem. Plasma Process. 11, 529–543.

Planche, M.P., Coudert, J.F., Fauchais, P., 1998. Velocity measurements for arc jets produced by a DC plasma spray torch. Plasma Chem. Plasma Process. 18, 263–283.

Sun, L., Berndt, C.C., Grey, C.P., 2003. Phase, structural and microstructural investigations of plasma sprayed hydroxyapatite coatings. Mater. Sci. Eng. A 360, 70–84.

Tsui, Y.C., Doyle, C., Clyne, T.W., 1998. Plasma sprayed hydroxyapatite coatings on titanium substrates, Part 1: mechanical properties and residual stress levels. Biomaterials 19, 2015–2029.

Vardelle, A., Fauchais, P., Vardelle, M., Mariaux, G., 2006. Direct current plasma spraying: diagnostics and process simulation. Adv. Eng. Mater. 8, 599–610.

Vilotijevic, M., Dacic, B., Bozic, D., 2009. Velocity and texture of a plasma jet created in a plasma torch with fixed minimal arc length. Plasma Sources Sci. Technol. 18, 8, 015016.

Wang, T., Reisel, A.D., Muller, E., 2004. Thermogravimetric and thermokinetic investigation of the dehydroxylation of a hydroxyapatite powder. J. Eur. Ceram. Soc. 24, 693–698.

Yang, C.Y., Lin, R.M., Wang, B.C., Lee, T.M., Chang, E., Hang, Y.S., Chen, P.Q., 1997. In vitro and in vivo mechanical evolutions of plasma-sprayed hydroxyapatite coatings on titanium implants: the effect of coating characteristics. J. Biomed. Mater. Res. 37, 335–345.

Yang, C.Y., Chang, E., 2001. Influence of residual stress on bonding strength and fracture of plasma-sprayed hydroxyapatite coatings on Ti–6Al–4V substrate. Biomaterials 22, 1827–1836.

Zheng, X., Huang, M., Ding, C., 2000. Bond strength of plasma-sprayed hydroxyapatite/Ti composite coatings. Biomaterials 21, 841–849.